Simple vortex states in films of type-I Ginzburg-Landau superconductor

Mark C. Sweeney and Martin P. Gelfand*
Department of Physics, Colorado State University, Fort Collins, Colorado 80523-1875, USA
(Received 26 June 2010; revised manuscript received 4 August 2010; published 8 December 2010)

Sufficiently thin films of type-I superconductor in a perpendicular magnetic field exhibit a triangular vortex lattice while thick films develop an intermediate state. To elucidate what happens between these two regimes, precise numerical calculations have been made within Ginzburg-Landau theory at $\kappa=0.5$ and 0.25 for a variety of vortex lattice structures with one flux quantum per unit cell. The phase diagram in the space of mean induction and film thickness includes a narrow wedge in which a square lattice is stable, surrounded by the domain of stability of the triangular lattice at thinner films/lower fields and, on the other side, rectangular lattices with continuously varying aspect ratio. The vortex lattice has an anomalously small shear modulus within and close to the square lattice phase. Solutions of the Ginzburg-Landau equations have been obtained by similar calculations for bulk systems and thin films with one vortex but two flux quanta per square or triangular unit cell. Primitive lattices of double-fluxoid vortices are thermodynamically unstable in bulk in both type-I and type-II superconductors, as expected. In type-I films these double-fluxoid lattices do not pre-empt the single-fluxoid lattice structures.

DOI: 10.1103/PhysRevB.82.214508 PACS number(s): 74.25.Uv, 74.20.De, 74.78.−w

I. INTRODUCTION

Thin films of a bulk type-I superconductor subject to a perpendicular magnetic field can behave like bulk type-II superconductors, in that they develop a vortex lattice in which each vortex carries a single-flux quantum. Pioneering theoretical treatments by Tinkham[1] and Maki[2] applied Ginzburg-Landau (GL) theory in the vicinity of the critical field where the order parameter vanishes and showed that the transition between normal state and superconducting state is continuous, just as in bulk type-II materials. Lasher[3] established that a triangular vortex lattice is favored near the upper critical field for sufficiently thin films and found that a sequence of vortex structures, starting with a square lattice and continuing to more complicated structures, develops with increasing thickness en route to the intermediate state. Some years later Callaway[4] pointed out that Lasher had not considered the most general Abrikosov-type solutions to the linearized GL equations, and he carried out a comprehensive analysis of the phase diagram for periodic vortex arrays close to the upper critical field. In the low-field limit, Pearl's[5,6] treatment of isolated vortices within London theory shows that vortices in a sufficiently thin film have a long-range repulsion; this repulsion should lead to the development of a triangular vortex lattice. Remarkably, the structure of the vortex phase diagram at intermediate magnetic field strengths, where solution of the full GL equations is required, has remained an open theoretical problem. That problem is partially solved in the present work.

On the experimental side, magnetic decoration experiments on type-I films of Pb, Sn, and In by Dolan and Silcox[7–9] in the mid-1970s could distinguish between lattices of single-fluxoid vortices (which appear to be disordered due to pinning), intermediate state flux structures, and what they referred to as "transitional" or "multifluxoid" structures. Within linearized GL theory one can construct a flux structure phase diagram with the GL parameter κ on one axis and the product of film thickness and the square root of the magnetic field on the other;[3] Dolan and Silcox's results were reasonably consistent with this phase diagram. However, there have been no experimental observations of the distinct single-fluxoid vortex lattice structures predicted by linearized GL theory. In fact it is not obvious whether the vortex structures found by Lasher and Callaway at intermediate thicknesses survive on reducing the magnetic field. The calculations within the full GL theory presented in this work offer detailed guidance for experimental studies of such structures in type-I films.

Interesting experimental results have also appeared at very low fields. Hasegawa *et al.*[10] applied electron holography to examine the magnetic field in the space above flux structures in Pb films. They found evidence for vortices with more than one flux quantum [which they denoted multiply quantized fluxes (MQF)-A] as well as flux structures that seemed more likely to be associated with normal regions of finite cross section (which they denoted MQF-B). "Multiply quantized" (also known as "giant") vortices are known to arise in various circumstances. Holes in a superconductor parallel to the field trap vortices with greater fluxoid number as their radii increase.[11] Arrays of holes (antidots) can trap multiple flux quanta per hole under appropriate conditions.[12] The repulsion of vortices from a film edge can lead to the formation of an equilibrium giant vortex in the center of a small, thin disk[13] and in other laterally confined geometries.[14] Metastable giant vortices develop in field cooling of small cylinders.[15] None of these seem relevant to the experiment of Hasegawa *et al.*, and the search for stable lattices of multiply quantized vortices in the phase diagram for type-I films without lateral confinement or defects was another motivation for the present work.

It is noteworthy that a bulk GL superconductor with $\kappa=1/\sqrt{2}$ and at the critical field exhibits massive (in fact complete) degeneracy with respect to vortex configurations.[16] Luk'yanchuk[17] has carried out a thorough analysis of corrections to the GL functional, together with deviations of κ and the magnetic field from their critical values, in breaking the

degeneracy. He noted that demagnetization effects also break the degeneracy but did no calculations along those lines. A film geometry corresponds to maximum demagnetization, so it may be interesting to compare the vortex phase diagram for films with $\kappa \approx 1/\sqrt{2}$ with the phase diagrams that follow from the analysis by Luk'yanchuk.

In this paper we take some initial steps toward filling out the magnetic flux structure phase diagram for the minimal model, isotropic Ginzburg-Landau theory, of thin film type-I superconductors. The competition between various phases is delicate, so precise and accurate free-energy calculations for different flux structures are necessary. Consequently, we have followed the approach pioneered by Brandt for vortex lattices in bulk[18] and, more recently, thin film[19] GL superconductors. The squared magnitude of the order parameter, the supervelocity, and the magnetic field are represented as linear combinations of appropriate basis functions. The GL equations then become a set of nonlinear equations which are solved by iteration.

The main text focuses on physics results from the calculations while the technical details are described in a series of Appendices A through D. Section II presents the nomenclature that will be used in connection with GL theory. Details of the method of minimizing the GL free energy for magnetic flux structures in films consisting of single-fluxoid vortices in lattices with one vortex per primitive cell are offered in Appendix A. We found that the functional form chosen for the magnetic field in Ref. 19 limits the accuracy of the calculated magnetic field and consequently the free energy, and we give a correct and computationally convenient alternative together with the necessary modifications to the algorithm for solving the associated nonlinear equations.

Section III presents the principal results of the calculations, which are based on evaluating the free energy for a large number of points in the space of vortex lattices structures, film thicknesses, and mean magnetic inductions. Phase diagrams, free energy densities, and vortex lattice shear moduli are given for $\kappa=0.5$ and 0.25. Other values of the GL parameter could have been considered but the calculations become significantly more challenging at smaller values of κ; and with results for just two values, some trends with variation in κ may be deduced. Section IV offers various decompositions of the free energy density to facilitate the physical interpretation of the flux structure phase diagram.

We have also extended Brandt's method to construct solutions of the GL equations for lattices of vortices which carry two flux quanta per vortex and one vortex per primitive cell. The formal developments for bulk superconductors, as well as some subtle but crucial implementation details, are presented in Appendices B and C, and the further developments for film geometry are briefly laid out in Appendix D.

It is well known that in bulk type-II superconductors double-fluxoid vortex lattices are thermodynamically unstable with respect to single-fluxoid vortex lattices—at least at low induction, thanks to the Matricon's[20] calculations for isolated vortices, and close to the upper critical field, as pointed out by Abrikosov.[21] In Sec. V we verify that it is true at arbitrary induction for $\kappa=1$, and present other results of calculations for lattices of double-fluxoid vortices in bulk type-II and type-I superconductors.

Section VI presents results for type-I films with double-fluxoid vortices. Those calculations cannot be converged over as broad a parameter range as those for either bulk geometries or for single-fluxoid vortex lattices and their physical implications are limited. Our main result is that the phase diagrams presented in Sec. III for single-fluxoid vortex lattices remain valid, in that the double-fluxoid lattices always have higher free energy in the range of parameters where we claimed that triangular, square, and rectangular lattices of single-fluxoid vortices were the equilibrium flux structures. In Sec. VII we summarize the results of our calculations and note their limitations, indicate some directions for future theoretical work, and offer suggestions for experiments.

A few remarks about alternative theoretical approaches to constructing magnetic flux structures for GL superconductors are in order before we proceed. Perhaps the most direct method is to start with the usual, nongauge-invariant form of the GL equations and construct a finite-difference approximation on a three-dimensional grid (except in cases where the system is translationally invariant along the direction of the magnetic field, for which a two-dimensional grid suffices). Because the equations are nonlinear an iterative solution is always required and the end result will depend on the initial values; a comparison of free energies can be carried out to determine the thermodynamically stable state. This approach has been applied to a variety of different problems.[12,14,22,23] An important aspect of this method is its generality: there are no symmetry constraints on either the physical system or the solutions of the equations. By imposing appropriate periodic boundary conditions it would be possible to construct periodic vortex lattice solutions that solve the problems treated in this paper. There are two significant advantages to the computational approach that we employ. First, the finite-difference approximation requires a grid that extends outside of the film for the vector potential, and so the number of variables would be significantly higher than for our method. Second, our method has an internal precision check, namely, inspection of the expansion coefficients corresponding to high wave numbers. For the finite-difference method it would be necessary to perform calculations at different grid spacing and extrapolate to zero grid spacing. The disadvantage of our method in comparison to finite-difference calculations is that we are limited to one vortex per primitive cell. It is conceivable that more complicated flux structures have lower free energy than the single-fluxoid triangular, square, and rectangular lattices where shown on the phase diagrams in Sec. III. We are confident that such is not the case, particularly at large mean inductions where our results are consistent with linearized GL theory; however, finite-difference calculations would be invaluable in establishing the large-thickness boundary of the rectangular phase and in determining what thermodynamically stable vortex lattices exist beyond it.

There are situations in which neither our method, nor finite-difference calculations, nor any other numerical approach to solving the full GL equations are appropriate. The flux structures experimentally observed in the intermediate state can be extremely complicated: see the recent work of Prozorov *et al.*[24,25] for some examples. In the theoretical

analysis of the intermediate state, physically approximate treatments of the GL equations such as the "current-loop" model[26] can be highly informative. However, in the regime of interest in the present work approximations of that sort are not necessary, and they would affect the calculations of phase diagrams and elastic moduli in an uncontrolled fashion.

II. GINZBURG-LANDAU THEORY

In this paper standard reduced units are employed in which lengths are multiples of the penetration depth λ, energy densities are multiples of $\mu_0 H_c^2$ (with H_c the thermodynamic critical field), and magnetic inductions are multiples of $\sqrt{2}\mu_0 H_c$. Note that in these units the upper critical mean induction is κ. We consider infinite films with $-d/2 < z < d/2$. The GL free energy can be expressed in gauge-invariant form (rather than in terms of the GL order parameter $\psi = fe^{i\varphi}$ and vector potential $\mathbf{A}$) by writing it in terms of the square of the order parameter, $\omega = f^2$, the supervelocity,

$$\mathbf{Q} = \mathbf{A} - \kappa^{-1} \nabla \varphi \tag{1}$$

and the deviation from mean induction,

$$\mathbf{b} = \mathbf{B} - \hat{\mathbf{z}}\bar{B}. \tag{2}$$

We let S denote both the unit-cell area and the unit cell itself, depending on context; for the former, $S = \Phi_0/\bar{B}$ with $\Phi_0 = 2\pi/\kappa$. The unit cell has primitive lattice vectors $\mathbf{R}_{10} = x_1\hat{\mathbf{x}}$, $\mathbf{R}_{01} = x_2\hat{\mathbf{x}} + y_2\hat{\mathbf{y}}$ and in those terms its area is $S = (\mathbf{R}_{10} \times \mathbf{R}_{01}) \cdot \hat{\mathbf{z}} = x_1 y_2$. The general reciprocal lattice vector is given by $\mathbf{K}_{mn} = 2\pi[my_2\hat{\mathbf{x}} + (mx_2 + nx_1)\hat{\mathbf{y}}]/S$. Note that the mean induction can be expressed as $\bar{B} = \frac{1}{S}\int_S dxdy \mathbf{B}(x,y,z) \cdot \hat{\mathbf{z}}$ for any value of z.

The free energy per unit volume of superconductor referenced to the normal state is

$$F = \frac{1}{Sd}\int_S dxdy \int_{-d/2}^{d/2} dz \left[-\omega + \frac{1}{2}\omega^2 + \frac{|\nabla\omega|^2}{4\kappa^2\omega} + \omega Q^2 + b^2 \right] + \frac{2}{Sd}\int_S dxdy \int_{d/2}^{\infty} dz [B^2 - \bar{B}^2], \tag{3}$$

where the contribution of the first two terms in the first integral is the condensation free energy F_{cond}, that of the next two terms is the kinetic energy of the supercurrent F_{kin}, that of the last term is the internal field energy F_{mag}, and that of the second integral is the stray field energy F_{stray}.

In order to determine the phase diagram we will compare the minimum F for different vortex lattice structures with the same value of $\bar{B}$ (and hence S). For a particular vortex lattice structure, minimizing the GL free energy with respect to variations in the order parameter yields the first GL equation

$$\frac{1}{2\kappa^2}\left(\nabla^2\omega - \frac{|\nabla\omega|^2}{2\omega} \right) = -\omega + \omega^2 + \omega Q^2. \tag{4}$$

The second GL equation is

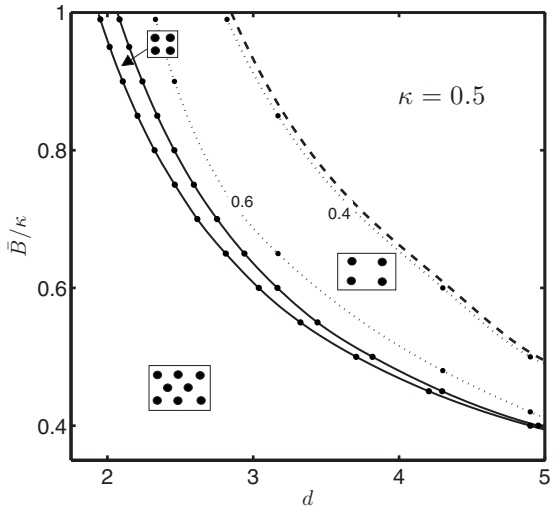

FIG. 1. Vortex lattice phase diagram for $\kappa = 0.5$. The triangular-square transition is discontinuous while the square-rectangular transition is continuous. Inside the rectangular phase, the dotted lines labeled 0.6 and 0.4 are contours of constant aspect ratio. The dashed line corresponds to the aspect ratio of 0.38, which is the smallest aspect ratio for which a rectangular lattice is stable at the upper critical field ($\bar{B}/\kappa = 1$), following Callaway (Ref. 4).

$$\nabla \times \mathbf{B} = -\omega\mathbf{Q}, \tag{5}$$

which is identical to Ampère's law in reduced units because the supercurrent $\mathbf{j}$ is

$$\mathbf{j} = -\omega\mathbf{Q}. \tag{6}$$

III. PHASE DIAGRAMS AND ELASTIC MODULI

We have carried out a series of calculations at various values of $\bar{B}$ and d, and for several kinds of vortex lattices including triangular, square, rectangular (at various aspect ratios) and two classes of oblique lattices which we will refer to as rhombohedral (which interpolate between triangular and square at fixed unit cell area, maintaining equality of the primitive vector lengths) and sheared triangular (which interpolate between triangular and rectangular at fixed unit cell area, keeping one primitive vector fixed). The vortex structure with lowest free energy turns out to be either triangular, square, or rectangular.

All of the results presented in this section are for $\kappa = 0.5$ and 0.25; even with just those two values for the GL parameter some trends with decreasing κ are evident. Calculations at small κ are considerably more challenging: we have not yet been able to obtained converged solutions at $\kappa = 0.1$.

Figures 1 and 2 show the resulting phase diagrams. The phases found at the critical field extend to lower fields but with the phase boundaries shifting to larger thicknesses as $\bar{B}$ is reduced. At sufficiently low $\bar{B}$ the interval of thickness where the square lattice is stable is seen to vanish on the $\kappa = 0.25$ phase diagram; and the same almost certainly holds for $\kappa = 0.5$ but at a lower value of $\bar{B}$ than we have considered. Contours of constant aspect ratio within the rectangular

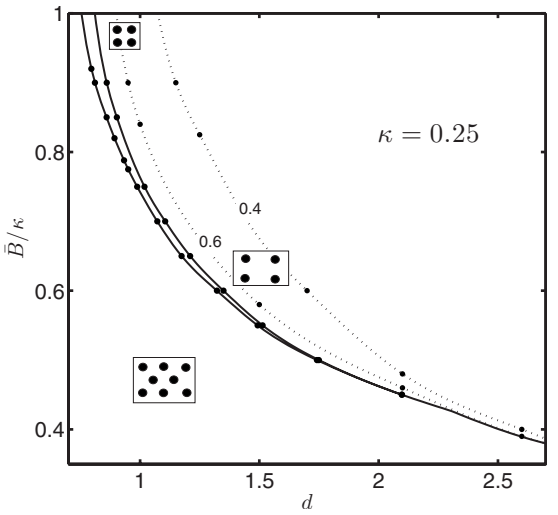

FIG. 2. Same as Fig. 1 but for κ=0.25. Note the critical endpoint for the square-rectangular transition at $d \approx 2.1$.

phase are shown as dotted lines. On the κ=0.5 phase diagram we have included a dashed line where we speculate that the rectangular phase ends and more complicated structures with more than one flux quantum per unit cell begin. At the critical field the location of that last phase boundary comes from the linearized GL analysis of Callaway;[4] and in drawing that line at lower fields we assume that the aspect ratio for the rectangular structure is constant along the boundary with the adjacent phase.

When the phase diagram from linearized GL theory is applied to interpret experiments (see, for example, Refs. 7–9) the phase boundaries at the critical field are extrapolated to lower field by assuming that $d\bar{B}^{1/2}$ is constant along the phase boundaries, as suggested by Lasher.[3] That is not a terrible approximation, but the numerical results are noticeably different, with the domain of stability of the triangular phase reduced compared to the linearized GL theory. The critical endpoint for the square to rectangular transition is a qualitative feature that only emerges from the full GL treatment.

It is interesting to look at the free energies that underlie the phase diagrams to see the scale of the free energy differences. In the lower panel of Fig. 3, F is presented as a function of mean induction for κ=0.5 and d=2.4 while Fig. 4 does the same for κ=0.25 and d=0.94 (the latter thickness is chosen so that the phase transitions in the two figures are at roughly the same values of $\bar{B}/\kappa$). The rhombohedral lattice free energies, not shown in those figures, are nearly degenerate with the free energies of square and triangular lattices at phase transition between them, and close to the transition their free energies almost linearly interpolate between square and triangular lattice free energies.

Shear moduli have been evaluated for the three lattice structures which appear on the phase diagram: see the upper panels of Figs. 3 and 4. For triangular lattices the only shear modulus is $c_{66}=\frac{1}{2}(c_{11}-c_{12})$. For square lattices there are two distinct types of shear, with moduli c_{66} and $\frac{1}{2}(c_{11}-c_{12})$: the former preserves equality of primitive lattice vector length

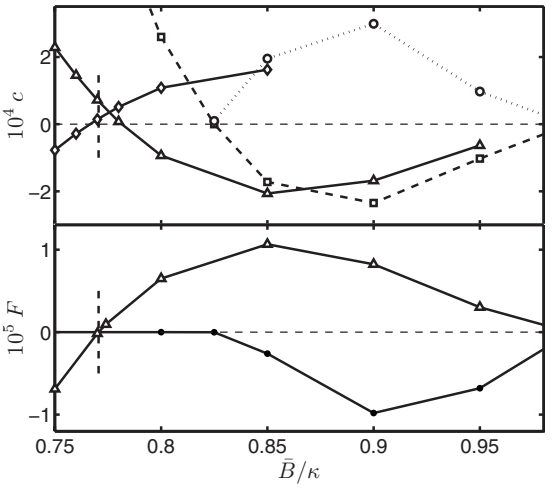

FIG. 3. Shear moduli and free energies per unit volume for triangular, square, and rectangular lattices, at κ=0.5 and d=2.4, for mean inductions around the domain of stability of the square lattice. Free energies are referenced to value for the square lattice; on that graph the triangular lattice values are the triangles and the minimum-F rectangular lattice values are the circles. The vertical dashed segments in both plots indicate the transition between triangular and square lattices, to make clear the discontinuity in shear modulus. On the shear modulus plot, triangles are c_{66} for the triangular lattice, diamonds are c_{66} for the square lattice, squares are $\frac{1}{2}(c_{11}-c_{12})$ for the square lattice, and circles are $\frac{1}{2}[(c_{11}+c_{22})/2-c_{12}]$ for the minimum-F rectangular lattice. Both free energy densities and shear moduli are in units of $\mu_0 H_c^2$.

while the latter preserves orthogonality of primitive lattice vectors. We present both on the figures because the latter vanishes at the continuous square-rectangular transition and the former is anomalously small at the discontinuous triangular-square transition. For the rectangular lattices we considered only the shear mode which preserves orthogonality of primitive lattice vectors; the corresponding modulus is $\frac{1}{2}[(c_{11}+c_{22})/2-c_{12}]$. In every case the shear modulus is calculated by evaluating the energy difference between the reference lattice structure and a slightly sheared lattice. One can

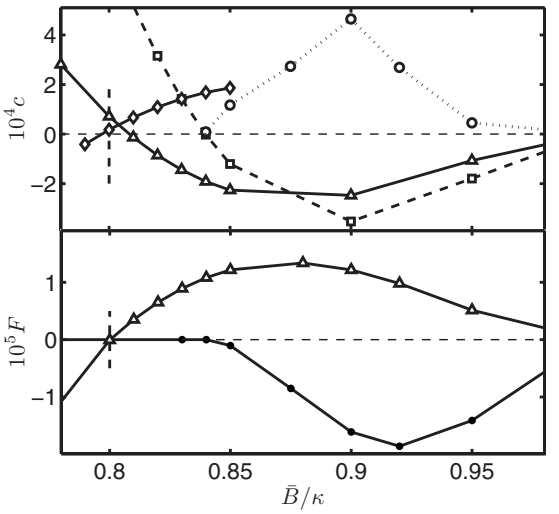

FIG. 4. Same as Fig. 3 but for κ=0.25 and d=0.94.

TABLE I. Film minus bulk free energy density terms for $\kappa=0.5$, $\bar{B}/\kappa=0.825$, and $d=2.0$.

	Triangular	Square
$10^4\Delta F_{\text{cond}}$	161.0	180.0
$10^4\Delta F_{\text{kin}}$	−116.0	−129.0
$10^4(\Delta F_{\text{mag}}+\Delta F_{\text{stray}})$	−25.5	−29.0

see in the figures the small domains of metastability for the triangular and square lattice phases. It is also apparent that the vortex lattices at these values of κ and d are anomalously soft for a wide range of mean inductions.

IV. FREE ENERGY DECOMPOSITIONS

The preceding section presented the main physical results of the calculations but further insight might be gained by comparing not just the free energy density for different lattice structures but also examining various parts of the free energy density. One decomposition is into the condensation, kinetic, and magnetic terms described following Eq. (3). Let us first consider $\kappa=0.5$, $\bar{B}/\kappa=0.825$, and $d=2.0$, which is in the triangular phase but not far from the square phase. For a bulk system at the same GL parameter and mean induction, the square lattice has lower free energy density than the triangular lattice. Why is the relative stability reversed in the film? In Table I we present the differences in free energy density components between the film and the bulk system for both triangular and square vortex lattices. The signs of all those differences may be understood as a consequence of suppression of the order parameter in the film compared to the bulk, and particularly a widening of the vortex cores associated with the spreading of the field lines near the film surfaces. However, the exchange of stability is a more subtle matter since that depends on the difference (triangular minus square lattice values) of those free energy density differences. Alternatively, we can compare the triangular and square lattice free energy density components for films of different thickness, as presented in Table II. It is then evident that with increasing thickness, the transition to the square vortex lattice is favored only by the condensation term.

We can also examine the z dependence of the free energy density, integrating in Eq. (3) only over x and y and dividing only by S to define $F(z)$. [F_{stray} is taken as a z-independent contribution to $F(z)$.] Figure 5 compares square and triangular vortex lattices for $\kappa=0.5$ just below the upper critical field for $d=1.5$, 2.0, and 2.5. The triangular lattice has lower total free energy only for $d=1.5$. However, in every case $F(z)$ is lower for the triangular lattice when $z\approx d/2$ and, with decreasing z, $F(z)$ decreases more rapidly for the square lattice than for the triangular lattice. Figure 5 is thus consistent with the interior of the film being more bulklike than the surface; and in fact $F(0)$ approaches F for a bulk system as d increases. The difference between $F(d/2)$ for triangular and square vortex lattices varies comparatively weakly with d. These features of $F(z)$ suggest a qualitative picture of the triangular-square lattice transition based on a competition between an interior region like that in bulk and a surface layer like that in an ultrathin ($d\ll\lambda$) film.

TABLE II. Differences in free energy density terms (triangular lattice minus square lattice) at $\kappa=0.5$ and $\bar{B}/\kappa=0.825$ for several values of d. Note that $\Delta F<0$ for $d=2.0$ but is positive at the other thicknesses.

d	2.0	2.33	2.6
$10^4\Delta F_{\text{cond}}$	−4.44	−2.64	−1.37
$10^4\Delta F_{\text{kin}}$	6.55	5.29	4.42
$10^4(\Delta F_{\text{mag}}+\Delta F_{\text{stray}})$	−2.31	−2.60	−2.81

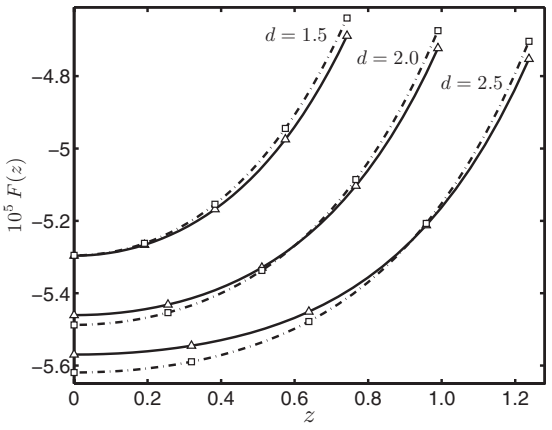

FIG. 5. Free energy density dependence on z for films of various thickness with $\kappa=0.5$ and $\bar{B}=0.99/\kappa$, for square and triangular vortex lattices (indicated by the symbols).

However, this picture is misses some important physics, which is revealed when $F(z)$ is decomposed along the lines of the condensation, magnetic, and kinetic terms. If the surface layers were ultrathin-film-like one would expect $F_{\text{cond}}(0)$ to be significantly different from $F_{\text{cond}}(d/2)$ since, as noted above, it is only the condensation term which favors the square lattice as the thickness is increased. Instead, we find that the condensation term is nearly independent of z, as is ω (as pointed out by Brandt for films of type-II superconductors[19]). F_{mag} is smaller at the surface, where the field lines spread out, than in the center of the film, which is contrary to the behavior of $F(z)$ as a whole, and therefore F_{kin} is mainly responsible for the z dependence seen in Fig. 5. In the regime explored in this paper, with the film thickness no more than a few multiples of either the penetration depth or the coherence length, it seems that no simple picture is adequate.

V. LATTICES OF DOUBLE-FLUXOID VORTICES IN BULK SUPERCONDUCTORS

We now turn to calculations for vortex lattices in which the vortices carry two flux quanta per unit cell. As noted in Sec. I, calculations for vortex lattice in bulk are a prerequisite for the corresponding calculations in film geometry. In this section we describe the bulk calculations. We are not

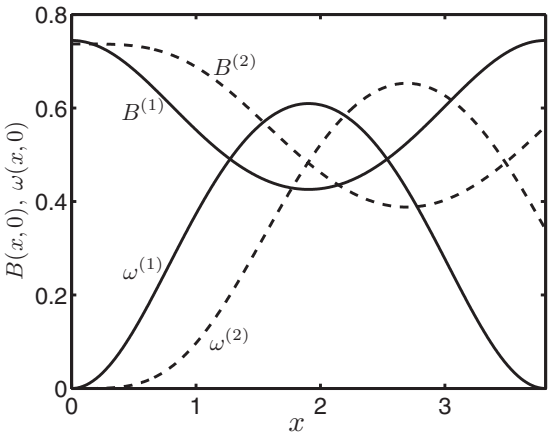

FIG. 6. Cross sections along $y=0$ of magnetic induction (curves decreasing from $x=0$) and squared order parameter (curves increasing from $x=0$) for double-fluxoid (dashed) and single-fluxoid (solid) triangular vortex lattices at the same parameters $\kappa=1$ and $\bar{B}=\mu_0 H_{c2}/2$. The horizontal axis label is written as as x/λ, even though $\lambda\equiv 1$ in the units used throughout this work, to emphasize that the same length scale is being used for both vortex lattices. The intervortex spacing for single-fluxoid vortices is 3.81λ and is greater by a factor of $\sqrt{2}$ for double-fluxoid vortices.

aware of previous calculations within nonlinear GL theory for lattices of multiple fluxoid vortices in bulk superconductors but since such flux structures were universally expected to be unstable with respect to the Meissner state or single-fluxoid vortex lattices there would have been little motivation to carry them out for their own sake.

The numerous technical developments required for these calculations are described in Appendices B and C. To illustrate the effectiveness of the calculational scheme described therein, we present results for $\kappa=1$ and $\kappa=1/2$ of triangular arrays of both double and single-fluxoid vortices.

For $\kappa=1$, Fig. 6 shows the order parameter and induction along a line connecting two adjacent vortices at $\bar{B}=\mu_0 H_{c2}/2$ for both double and single-fluxoid vortices. As one would expect, the cores of double-fluxoid vortices are wider than those of single-fluxoid vortices. Figure 7 presents

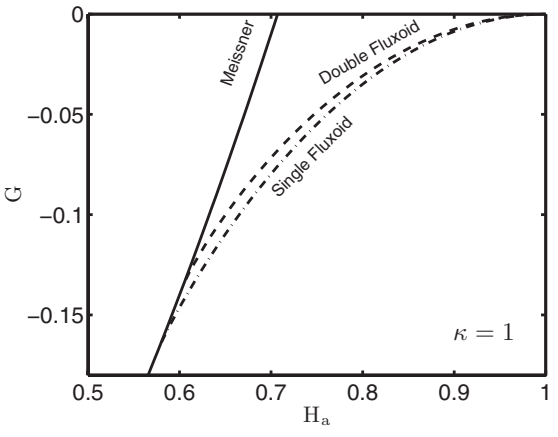

FIG. 7. Gibbs free energy densities, referenced from the normal state, as a function of applied field at GL parameter $\kappa=1$ for bulk superconductor.

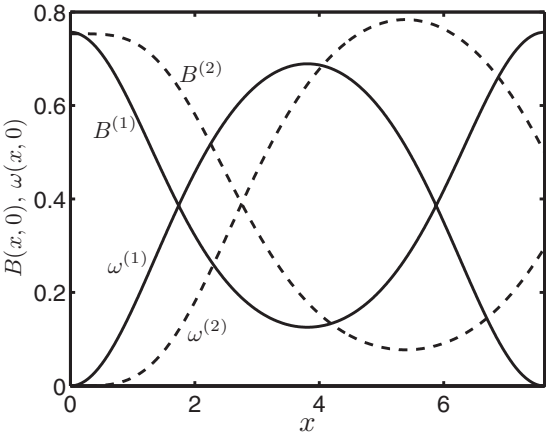

FIG. 8. Same as Fig. 6 but for $\kappa=1/2$. The intervortex spacing for single-fluxoid vortices is 7.62λ.

the magnetic Gibbs free energy density $G=F-\mathbf{H}_a\cdot\mathbf{B}$ in the full range of applied fields $H_{c1}\leq H_a\leq H_{c2}$ for triangular lattices of single and double-fluxoid vortices. The applied field H_a is calculated in the same manner as in Refs. 27 and 28, based on the virial theorem of Doria *et al.*[29] These calculations confirm the universal expectation that double-fluxoid vortex lattices are thermodynamically unstable in bulk type-II superconductors at arbitrary applied field.

For $\kappa=1/2$ the corresponding results are shown in Figs. 8 and 9. Neither of the vortex lattices are thermodynamically stable at any applied field, as expected for a bulk type-I superconductor; below the thermodynamic critical field the Meissner state is stable. What might not have been expected is that the vortex lattices have a higher Gibbs free energy than the *normal* state. In addition, $\partial^2 G/\partial H_a^2>0$, which is inconsistent with a thermodynamically stable homogeneous state, but not a surprise since the mixed state is inhomogeneous. Nonetheless, the magnetic induction and order parameter profiles associated with these vortex lattices are entirely unremarkable, and serve well as initial values for calculations in film geometry.

VI. LATTICES OF DOUBLE-FLUXOID VORTICES IN FILMS

Solutions of the GL equations in film geometry with lattices of double-fluxoid vortices may be obtained by combin-

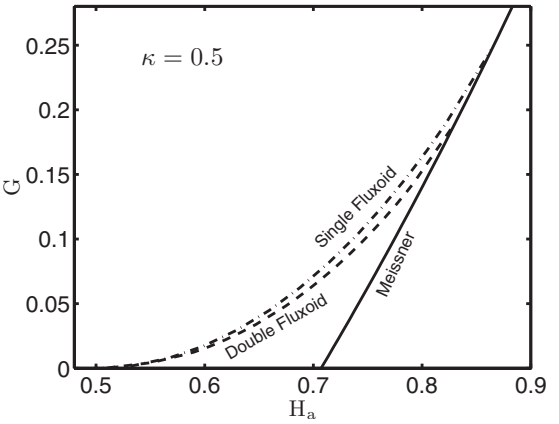

FIG. 9. Same as Fig. 7 but for $\kappa=1/2$.

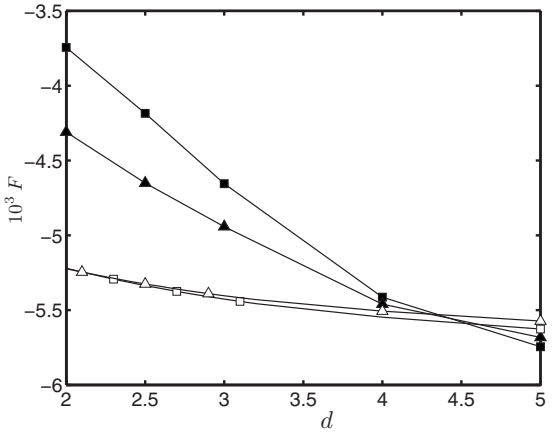

FIG. 10. Free energy densities of several vortex lattice structures as a function of film thickness at mean induction $\bar{B}=0.9\mu_0 H_{c2}$ for $\kappa=1/2$. Triangle symbols are for triangular lattices and square symbols are for square lattices; open symbols are for single-fluxoid vortices and solid symbols for double-fluxoid vortices.

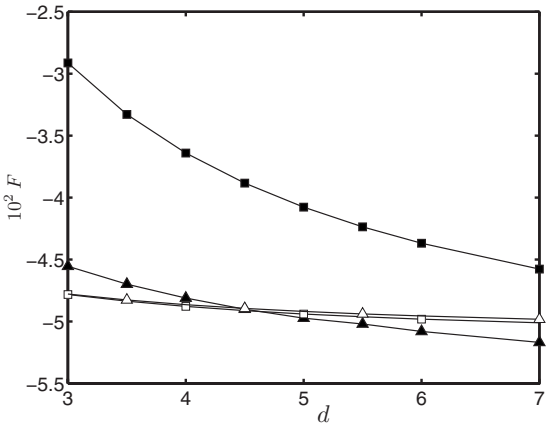

FIG. 11. Same as Fig. 10 but for mean induction $\bar{B}=0.7\mu_0 H_{c2}$.

ing the developments of Appendices A and B. The relevant formulas are presented in Appendix D.

Our results in film geometry for double-fluxoid vortex lattices are very limited compared to those for single-fluxoid vortices for several reasons. The calculations for double-fluxoid vortex lattices converge more slowly, by roughly a factor of 5, than for single-fluxoid vortices. (That is not unexpected, given that the same holds for the bulk calculations.) Furthermore, there is a narrower range of parameters in which we have been able to obtained converged results at all. Surprisingly, we have encountered difficulties with mean inductions too close to the upper critical value, for which the single-fluxoid vortex lattice calculations readily converge. But the main issue is that these calculations have much less physical significance than their single-fluxoid analogs. In the portion of parameter space where states of one flux quantum per primitive cell are not the equilibrium flux configuration, there are many competing states, and those with one double-fluxoid vortex per primitive cell form a small subset. In fact, Callaway's results[4] suggest that such states are never the global free energy minima close to the upper critical field. Consequently there is no reason to carry out extensive calculations to arrive at a phase diagram for double-fluxoid vortex lattices analogous to Fig. 1. What we can do, instead, is offer some further support for the phase diagram of Fig. 1 by showing that double-fluxoid vortex lattices have greater free energy than single-fluxoid vortex lattices in the region of parameter space we claim that the latter are stable.

Figures 10 and 11 present free energy densities referenced to the normal state as a function of film thickness for a $\kappa=1/2$ superconductor at mean inductions which are 90% and 70%, respectively, of the critical value. Triangular and square lattices of single and double-fluxoid vortices are compared. (The minimum free energy rectangular lattices of single-fluxoid vortices lie close enough to the square lattices for this purpose.) At 90% of the critical $\bar{B}$, the speculated boundary between rectangular vortex lattice and more complicated structures is at $d\approx 3.2$ while a double-fluxoid structure does not yield a lower free energy than the single-fluxoid square lattice until $d>4.5$. At 70% of the critical $\bar{B}$, the corresponding values are $d\approx 4.0$ and $d>4.5$. If that trend continues, it is possible that at sufficiently small $\bar{B}$ and large d the phase diagram, Fig. 1, will require revision; however we have not been able to obtain converged double-fluxoid vortex lattice solutions at low enough mean induction to make a definite claim.

VII. CONCLUSIONS

We have improved and extended Brandt's method[19] for solving the GL equations for thin-film superconductors in perpendicular magnetic fields, and applied it to a series of calculations for various flux structures with one single-fluxoid vortex per primitive cell in type-I superconductor films of intermediate (several times the penetration depth) thickness. The phase diagrams presented in Sec. III are a significant step beyond the linearized theory toward the development of an accurate equilibrium flux structure phase diagram for films of type-I GL superconductors. The results suggest that nontriangular (square and rectangular) single-fluxoid vortex lattice structures can be thermodynamically stable at mean inductions well below the upper critical value.

The anomalous softness of the vortex lattice in and near the domain of stability for the square vortex lattice offers hope that some features of the theoretical phase diagram might be observed in critical current measurements, in the form of "peak effects"[30] well below the upper critical field. Such measurements are much simpler to carry out than any vortex imaging experiment. However, quantitative comparison between the theoretical phase diagrams and experimental results may be complicated by thermal fluctuations[31] and other effects which are unaccounted for in the minimal GL free energy.

More fully developed phase diagrams would require similar calculations for structures with more that one flux quantum per primitive cell. We have made progress in that direction with our results for primitive lattices of double-fluxoid vortices, which are degenerate cases of two flux quanta per primitive cell. The complexity of the solution for even these

special cases, as detailed in Appendices B through D, suggests the difficulty of treating the general case. So far our attempts at Ansätze and iterative algorithms for two single-fluxoid vortices in a unit cell have failed to converge to physically reasonable solutions.

The only definite conclusions that we have been able to draw from the double-fluxoid vortex calculations concern bulk type-II superconductors. As long expected, but never explicitly demonstrated, lattices of double-fluxoid vortices have higher magnetic Gibbs free energy than lattices of single-fluxoid vortices at all values of applied field. For films, all we are able to state is that the calculations for double-fluxoid lattice structures do not lead us to modify the phase diagrams presented in Sec. III.

ACKNOWLEDGMENTS

We have benefited from many conversations with Stuart Field. This work has been supported by the National Science Foundation through Grant No. DMR 94-57928.

APPENDIX A: SINGLE-FLUXOID VORTEX LATTICE CALCULATIONS IN FILM GEOMETRY

A key step in Brandt's approach[19] is to decompose the supervelocity as

$$\mathbf{Q} = \mathbf{Q}_A + \mathbf{q}, \tag{A1}$$

where $\mathbf{Q}_A$ is the supervelocity of the Abrikosov solution corresponding to the given vortex lattice, which satisfies

$$\nabla \times \mathbf{Q}_A = \left[\bar{B} - \Phi_0 \sum \delta_2(\mathbf{r}_\perp - \mathbf{R}_{\text{vortex}})\right]\hat{\mathbf{z}}, \tag{A2}$$

where $\mathbf{r}_\perp = (x,y)$, δ_2 is the two-dimensional Dirac delta function, and the sum runs over all vortices. Inside the film,

$$\mathbf{b} = \nabla \times \mathbf{q}. \tag{A3}$$

With the definitions and relations from Sec. II and just above, the problem is to determine ω, $\mathbf{q}$, and $\mathbf{b}$ that minimize the free energy. Brandt's Ansatz for these fields is as follows:

$$\omega(\mathbf{r}) = \sum_{\mathbf{K}_\perp, K_z} a_{\mathbf{K}_\perp K_z}[1 - \cos \mathbf{K}_\perp \cdot \mathbf{r}_\perp]\cos K_z z, \tag{A4}$$

$$\mathbf{q}(\mathbf{r}) = \sum_{\mathbf{K}_\perp, K_z} b_{\mathbf{K}_\perp K_z} \frac{\hat{\mathbf{z}} \times \mathbf{K}_\perp}{K_\perp^2} \sin \mathbf{K}_\perp \cdot \mathbf{r}_\perp \cos K_z z, \tag{A5}$$

$$b_z(\mathbf{r}) = \sum_{\mathbf{K}_\perp, K_z} b_{\mathbf{K}_\perp K_z} \cos \mathbf{K}_\perp \cdot \mathbf{r}_\perp \cos K_z z, \tag{A6}$$

$$\mathbf{b}_\perp(\mathbf{r}) = \sum_{\mathbf{K}_\perp, K_z} b_{\mathbf{K}_\perp K_z} \frac{\mathbf{K}_\perp K_z}{|\mathbf{K}_\perp|^2} \sin \mathbf{K}_\perp \cdot \mathbf{r}_\perp \sin K_z z. \tag{A7}$$

Here $\mathbf{K}_\perp$ is the set of reciprocal lattice vectors, excluding the origin, and $K_z = (2\pi/d)n$ with n running over the whole numbers. Several features of this Ansatz are worth noting. Only two sets of expansion coefficients, $a_{\mathbf{K}_\perp K_z}$ and $b_{\mathbf{K}_\perp K_z}$, are required because $\mathbf{b}$ and $\mathbf{q}$ are linked by Eq. (A3). The periodicity of ω combined with the quadratic behavior of ω near the vortices suggests the form of expansion for the $\mathbf{r}_\perp$ dependence in Eq. (A4) while the boundary condition for the order parameter at a superconductor-insulator interface makes the cosine expansion natural for the z dependence. Equation (A5) leads to supercurrents with, as one would anticipate, only in-plane components, as well as with the appropriate periodicity and behavior near vortex lines. The motivation for the z dependence of the expansions for $\mathbf{b}$ and $\mathbf{q}$ is that $\mathbf{q}$ and b_z are even functions of z while $\mathbf{b}_\perp$ is an odd function.

Inserting Eqs. (A4) and (A5) into the first GL equation leads to coupled nonlinear equations for the expansion coefficients $a_{\mathbf{K}_\perp K_z}$ and $b_{\mathbf{K}_\perp K_z}$ which can be readily cast in the form of equations for the $a_{\mathbf{K}_\perp K_z}$ suitable for solution by iteration: see Eq. (A15) below. More equations must come from the second GL equation inside the film, together with $\nabla \times \mathbf{b} = 0$ outside the film and the boundary conditions on the induction. The induction above the film satisfies

$$B_z = \bar{B} + \sum_{\mathbf{K}_\perp} b^s_{\mathbf{K}_\perp} \cos \mathbf{K}_\perp \cdot \mathbf{r}_\perp e^{-K_\perp (z - d/2)}, \tag{A8}$$

$$\mathbf{B}_\perp = \sum_{\mathbf{K}_\perp} b^s_{\mathbf{K}_\perp} \frac{\mathbf{K}_\perp}{K_\perp} \sin \mathbf{K}_\perp \cdot \mathbf{r}_\perp e^{-K_\perp (z - d/2)} \tag{A9}$$

and the continuity-of-B_z boundary condition may be expressed as

$$b^s_{\mathbf{K}_\perp} = \sum_{K_z} b_{\mathbf{K}_\perp K_z} \cos dK_z/2. \tag{A10}$$

It is convenient to derive the equations for the expansion coefficients by direct minimization of the free energy (including the stray field energy) with respect to the $b_{\mathbf{K}_\perp K_z}$, which leads to Eqs. (19)–(23) of Ref. 19.

In order to carry out a calculation of the expansion coefficients it is necessary to truncate the expansion, setting $a_{\mathbf{K}_\perp K_z}$ and $b_{\mathbf{K}_\perp K_z}$ to zero for $\mathbf{K}_\perp K_z$ outside some range. It is also necessary to approximate the integrals that appear in the iteration equations as finite sums. Those integrals arise from applying orthogonality relations and, ideally, the coefficient truncation and numerical integration could be done consistently so that the trigonometric functions retained in the expansion are orthogonal with respect to the numerical integration. This is done naturally for the z coordinates of the integration, by making the simplest choice of uniform spacing. In the xy plane Brandt employs a rectangular grid for integration but a circular domain for the allowed $\mathbf{K}_\perp$ values. Though a rectilinear domain for $\mathbf{K}_\perp$ would be more consistent we have followed Brandt's choice, on the grounds that when $K_\perp$ is large the expansion coefficients ought to be small.

What is there to object to in the method described above? In brief, Eq. (A5) [and its corollaries Eqs. (A6) and (A7)] impose periodic boundary conditions in the z direction which are not physically appropriate. According to Eq. (A7), as the film surface is approached from within, $\mathbf{b}_\perp(\mathbf{r}) \to 0$. This leads to a discontinuity in $\mathbf{b}_\perp$ across the film boundary, as can be seen from Eq. (A9), which by Ampère's law implies a

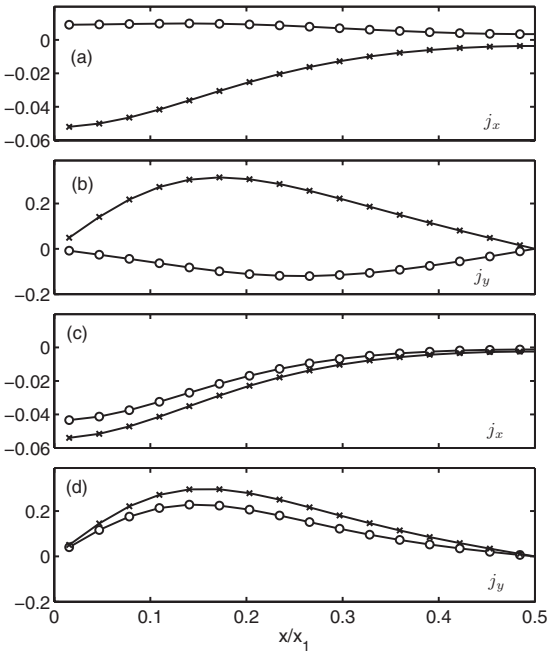

FIG. 12. Supercurrent density components j_x and j_y calculated from $-\omega\mathbf{Q}$ (crosses) and $\nabla\times\mathbf{B}$ (circles) from solutions by the method of Ref. 19 for a system with $\kappa=0.5$, $\bar{B}=0.4/\kappa$, $d=4.3$, and a $32\times13\times9$ grid for real-space sampling. The vortex lattice is triangular, with one primitive translation being $x_1\hat{x}$. In these plots $y=0.017x_1$, with $z=0.89d/2$ for (a) and (b) and $z=0$ for (c) and (d).

sheet current density at the film surface which is inconsistent with the GL (or even London) theory description of a superconductor.

The consequences of this flaw in the Ansatz are surprisingly difficult to see—no clear sign of it appears in the results presented by Brandt in Ref. 19, many of which we reproduced independently. When we implemented that method the first suggestion of a problem came when we compared two calculations of the supercurrent which should have given the same results, namely, $\mathbf{j}=-\omega\mathbf{Q}$ and $\mathbf{j}=\nabla\times\mathbf{B}=\nabla\times\mathbf{b}$. An example is shown in Fig. 12, for a system at fairly low mean induction. Note that the supercurrent calculated according to $\nabla\times\mathbf{B}$ actually circulates in the wrong direction for some values of z. A hint that the problem was the form of the z dependence in Eqs. (A5)–(A7), and not simply an error in our implementation as we first supposed, was that the disagreement become more evident as the maximum value of K_z was increased.

Our solution is to replace the cosine expansion for the z dependence of $\mathbf{q}$ with an expansion in terms of Legendre polynomials of even order since the latter form a complete, orthogonal set of even functions over a finite interval that allow for nonzero derivatives at the ends of the interval. Instead of Eqs. (A5)–(A7), take

$$\mathbf{q}(\mathbf{r})=\sum_{\mathbf{K}_\perp,l} b_{\mathbf{K}_\perp l}\frac{\hat{\mathbf{z}}\times\mathbf{K}_\perp}{K_\perp^2}\sin\mathbf{K}_\perp\cdot\mathbf{r}_\perp P_{2l}(2z/d), \quad \text{(A11)}$$

$$b_z(\mathbf{r})=\sum_{\mathbf{K}_\perp,l} b_{\mathbf{K}_\perp l}\cos\mathbf{K}_\perp\cdot\mathbf{r}_\perp P_{2l}(2z/d), \quad \text{(A12)}$$

$$\mathbf{b}_\perp(\mathbf{r})=\sum_{\mathbf{K}_\perp,l} b_{\mathbf{K}_\perp l}\frac{-\mathbf{K}_\perp}{K_\perp^2}\sin\mathbf{K}_\perp\cdot\mathbf{r}_\perp\frac{2}{d}P'_{2l}(2z/d). \quad \text{(A13)}$$

There is an additional benefit of the Legendre polynomial expansion for the accuracy of the calculations. A numerical scheme for z integration which maintains orthogonality of the Legendre polynomials is appropriate for the iterative calculation of the b coefficients, namely, Gauss-Legendre quadrature. The abscissas for Gauss-Legendre quadrature are at zeros of P_n (where n is larger than the highest order used in the Ansatz), and these zeros are more numerous near the film surfaces where the most rapid changes occur for $\mathbf{b}$ and $\mathbf{q}$. Finally, the Legendre polynomials are optimal for our purposes, compared to other sets of polynomials, because they are orthogonal with respect to a constant weight function, just like the trigonometric functions.

We now present the full scheme for generating solutions to the GL equations for films. We use $\langle\cdots\rangle_{\mathrm{U}}$ to denote the volume average over a unit cell by numerical quadrature in which the z abscissas are uniformly spaced while $\langle\cdots\rangle_{\mathrm{G}}$ is the same, except it employs Gauss-Legendre quadrature for the z coordinate. Angle brackets without a subscript refer to an analytic expression for the volume average over the unit cell. Before beginning the iterative calculations a set of initial $a_{\mathbf{K}_\perp K_z}$ and $b_{\mathbf{K}_\perp l}$ coefficients must be chosen; we will discuss that choice following the iteration scheme.

For the order parameter coefficients we use Brandt's iteration scheme, without modification, but for completeness we include it here. Defining

$$g=|\nabla\omega|^2/4\kappa^2\omega \quad \text{(A14)}$$

the first GL equation leads to the iteration

$$a_{\mathbf{K}_\perp K_z}:=\frac{4\langle(\omega^2-2\omega+\omega Q^2+g)\cos\mathbf{K}_\perp\cdot\mathbf{r}_\perp\cos K_z z\rangle_{\mathrm{U}}}{(\delta_{K_z,0}+1)[(K_\perp^2+K_z^2)/2\kappa^2+1]}. \quad \text{(A15)}$$

This is always followed by an iteration to minimize F by multiplying all the $a_{\mathbf{K}_\perp K_z}$ by the same factor,

$$a_{\mathbf{K}_\perp K_z}:=a_{\mathbf{K}_\perp K_z}\langle\omega-g-\omega Q^2\rangle_{\mathrm{U}}/\langle\omega^2\rangle_{\mathrm{U}}. \quad \text{(A16)}$$

This step was introduced by Brandt in solving the GL equations in bulk superconductors; if omitted, the calculations generally do not converge.

Next comes the iteration for the $b_{\mathbf{K}_\perp l}$. Our modification of the expansions for $\mathbf{b}$ and $\mathbf{q}$ require corresponding changes to the iteration scheme compared to Ref. 19. It is convenient to construct some auxiliary quantities such as the stray-field expansion coefficients

$$b^{\mathrm{s}}_{\mathbf{K}_\perp}=\sum_l b_{\mathbf{K}_\perp l} \quad \text{(A17)}$$

[compare Ref. 19, Eqs. (10) and (21)]; a quantity that arises from $\partial\langle\omega Q^2\rangle/\partial b_{\mathbf{K}_\perp l}$,

$$D_{\mathbf{K}_\perp l}=\langle\omega[Q_yK_x-Q_xK_y]\sin\mathbf{K}_\perp\cdot\mathbf{r}_\perp P_{2l}(2z/d)\rangle_{\mathrm{G}} \quad \text{(A18)}$$

[compare Ref. 19, Eqs. (20) and (22)]; and

$$S_{\mathbf{K}_\perp l} = \sum_{l'=0}^{l} b_{\mathbf{K}_\perp l'} 2l'(2l'+1) + \sum_{l'=l+1} b_{\mathbf{K}_\perp l'} 2l(2l+1), \tag{A19}$$

which appears in

$$\partial\langle b^2\rangle/\partial b_{\mathbf{K}_\perp l} = 2S_{\mathbf{K}_\perp l}/(dK_\perp)^2 + b_{\mathbf{K}_\perp l}/(4l+1). \tag{A20}$$

These last two expressions are rather more complicated than the corresponding Eq. (19) of Ref. 19 because, unlike sines and cosines, the P'_{2l} are not orthogonal. The second sum in Eq. (A19) is finite on account of the truncation of the expansion.

With these definitions the revised iteration scheme is

$$b_{\mathbf{K}_\perp l} := \frac{-2S_{\mathbf{K}_\perp l} - 2D_{\mathbf{K}_\perp l} - 2K_\perp b^{\mathrm{s}}_{\mathbf{K}_\perp}/d + c\langle\omega\rangle b_{\mathbf{K}_\perp l}}{K_\perp^2/(4l+1) + c\langle\omega\rangle}, \tag{A21}$$

where the constant c and the order parameter mean $\langle\omega\rangle = \Sigma_{\mathbf{K}_\perp} a_{\mathbf{K}_\perp 0}$ are included to stabilize the iterations [compare Ref. 19, Eq. (23)].

The algorithm is started with an initial guess for the $a_{\mathbf{K}_\perp K_z}$ and $b_{\mathbf{K}_\perp l}$ coefficients. Convergence to the physical solutions is not guaranteed, and in fact it is essential to have good initial values. We used bulk solutions[27] as initial values for $a_{\mathbf{K}_\perp 0}$ and $b_{\mathbf{K}_\perp 0}$, with the other coefficients initially zero. (The bulk solutions themselves require initial values for $a_{\mathbf{K}_\perp 0}$; for those, which can be taken from solutions of the linearized GL equations which are known for all lattice structures with one vortex per primitive cell.[32])

One cycles through Eqs. (A15), (A16), and (A21) until F has converged to an absolute tolerance of 1×10^{-10} or better, which typically requires about 200 iterations. This is slower convergence than is achieved with the cosine Ansatz for the z dependence for the supervelocity. A possibly related matter is that we have not found a suitable expression for the "stabilizer" c that works well—large enough to maintain stability of the iteration scheme, small enough to allow for reasonably quick convergence—over the entire range of parameters that we have studied. What we do instead is to adjust c during the iteration cycle by monitoring the evolution of F_{mag} and F_{stray} because when either of those field energies increases strongly it is a sign that an instability is developing. An algorithm that works reliably is that when either F_{mag} and F_{stray} increases by more than 50% following Eq. (A21) then c is multiplied by 10 and the $b_{\mathbf{K}_\perp l}$ iteration is rerun; independently, every 30 iterations c is divided by 2.

Although our calculations do not converge as rapidly as those reported in Ref. 19 they always lead to solutions with lower free energies, typically by 0.5% or less (with the same number of coefficients included in both calculations). These small differences are enough to produce noticeable changes in the phase boundaries. Our calculations also have the appealing feature that increasing the l cutoff for the $b_{\mathbf{K}_\perp l}$ always gives an improved solution; the same is not true of increasing the K_z cutoff for the $b_{\mathbf{K}_\perp K_z}$. Repeating the calculations presented in Fig. 12 yields supercurrent densities from $-\omega\mathbf{Q}$ and $\nabla\times\mathbf{B}$ which are nearly coincident, and which are close to the $-\omega\mathbf{Q}$ values displayed in that figure.

APPENDIX B: GENERALIZING BRANDT'S METHOD TO DOUBLE-FLUXOID VORTEX LATTICES

Consider a vortex in which the phase of the order parameter changes by $2\pi p$ on circling the vortex core. If that core is at the origin, then the order parameter behaves as $\psi \sim r^p e^{ip\theta}$ as $r\to0$ (see, for example, Tinkham,[33] Sec. 5.1) and the modulus squared order parameter as $\omega \equiv |\psi|^2 \sim r^{2p}$. Now focus on the $p=2$ case. Brandt suggests[27] that for a lattice with one vortex per primitive cell we adopt the Ansatz

$$\omega(\mathbf{r}) = \sum_{\mathbf{K}} a_{\mathbf{K}}[1-\cos(\mathbf{K}\cdot\mathbf{r})]^2 \tag{B1}$$

in which $\mathbf{r}$ is a two-dimensional vector and $\mathbf{K}$ runs over reciprocal lattice vectors excluding the origin. This form satisfies the requirements of periodicity and fourth-power behavior near vortex cores. It turns out to be useful to express this with only first powers of cosines, as

$$\omega(\mathbf{r}) = \sum_{\mathbf{K}} a_{\mathbf{K}}\left[\frac{3}{2} - 2\cos(\mathbf{K}\cdot\mathbf{r}) + \frac{1}{2}\cos(2\mathbf{K}\cdot\mathbf{r})\right]. \tag{B2}$$

In a bulk superconductor $\mathbf{B}(\mathbf{r}) = B(\mathbf{r})\hat{\mathbf{z}}$. For small r the induction satisfies $B(\mathbf{r}) \approx B(0) - \frac{1}{2\kappa}\omega(\mathbf{r})$, so $B(0) - B(r) \sim r^4$. The small-r behavior suggests the following form for the deviation from mean induction, $b(\mathbf{r}) = B(\mathbf{r}) - \bar{B}$:

$$b(\mathbf{r}) = \sum_{\mathbf{K}} b_{\mathbf{K}}\left[2\cos(\mathbf{K}\cdot\mathbf{r}) - \frac{1}{2}\cos(2\mathbf{K}\cdot\mathbf{r})\right]. \tag{B3}$$

The supervelocity is decomposed as $\mathbf{Q}(\mathbf{r}) = \mathbf{Q}_A(\mathbf{r}) + \mathbf{q}(\mathbf{r})$, where $\mathbf{Q}_A$ is the supervelocity in the Abrikosov limit, satisfying $\nabla\times\mathbf{Q}_A(\mathbf{r}) = [\bar{B} - 2\Phi_0\delta(\mathbf{r})]\hat{\mathbf{z}}$, and the deviation from the Abrikosov form satisfies

$$\mathbf{q}(\mathbf{r}) = \sum_{\mathbf{K}} b_{\mathbf{K}} \frac{\hat{\mathbf{z}}\times\mathbf{K}}{|\mathbf{K}^2|}\left[2\sin(\mathbf{K}\cdot\mathbf{r}) - \frac{1}{4}\sin(2\mathbf{K}\cdot\mathbf{r})\right]. \tag{B4}$$

Since the GL equations and their solutions are independent of z in the bulk, it is possible to obtain iterative expressions for both the $a_{\mathbf{K}}$ and the $b_{\mathbf{K}}$ directly from the GL equations, rather than extremalizing the GL free energy as was done for $b_{\mathbf{K}}$ in films following Ref. 19.

The first GL equation leads to an iterative equation for $a_{\mathbf{K}}$. Following Brandt,[27] we obtain

$$a_{\mathbf{K}} := \frac{2\kappa^2}{|\mathbf{K}|^2 + 2\kappa^2}\langle(-2\omega + \omega^2 + \omega|\mathbf{Q}|^2 + g)\cos\mathbf{K}\cdot\mathbf{r}\rangle + \frac{1}{4}a_{\mathbf{K}/2}. \tag{B5}$$

If $\mathbf{K}/2$ is not a reciprocal lattice vector then $a_{\mathbf{K}/2} \equiv 0$; we will refer to such reciprocal lattice vectors as "fundamentals." Equation (B5) should be compared with the corresponding relation for single-fluxoid vortices, Eq. (11) in Ref. 27: the only differences are the existence of the second term and a factor of 2 in the first term.

The next step in the iterative scheme, as in Ref. 27, is to rescale all of the $a_{\mathbf{K}}$ so as to minimize F. This goes through without modification.

Finally, iterative equation for $b_{\mathbf{K}}$ is

$$b_{\mathbf{K}} := -\frac{\langle[(\omega-\langle\omega\rangle)B(\mathbf{r})+(\nabla\omega\times\mathbf{Q})\cdot\hat{z}]\cos\mathbf{K}\cdot\mathbf{r}\rangle}{|\mathbf{K}|^2+\langle\omega\rangle}+\frac{1}{4}b_{\mathbf{K}/2} \tag{B6}$$

and if $\mathbf{K}$ is a fundamental then $b_{\mathbf{K}/2}\equiv 0$.

The GL equations are solved, in principle, by cycling through the three steps in the iterative scheme until the coefficients converge to the desired level of precision. In practice we find that the equations as written do not usually converge to a physical solution; however, by "mixing" the $a_{\mathbf{K}}$ that comes out of Eq. (B5) with the value from the prior iteration [and likewise for the $b_{\mathbf{K}}$ produced by Eq. (B6)] the convergence of the algorithm is much improved. We have not attempted to determine optimal mixing parameters but taking 90% of the prior iteration plus 10% of the current iteration has been sufficient.

Even with mixing, it is crucial to have a good initial guess for the $a_{\mathbf{K}}$ and $b_{\mathbf{K}}$. Brandt demonstrated[27] that the solution of the linearized GL equations for the $a_{\mathbf{K}}$, together with $b_{\mathbf{K}}=0$ for all $\mathbf{K}$, serves well for the initial values for single-fluxoid vortex lattices at any $\bar{B}$. For type-II superconductors the same holds true for double-fluxoid vortex lattices; however, for $\kappa<1/\sqrt{2}$ that choice of initial values does not always lead to a converged solution. For type-I superconductors we have found it necessary to first carry out calculations close to the upper critical mean induction and then gradually reduce $\bar{B}$, using the results of the $a_{\mathbf{K}}$ and $b_{\mathbf{K}}$ for the larger $\bar{B}$ as initial values for the subsequent calculation. The initial values for the calculations at the largest $\bar{B}$ are taken from solutions to the linearized first GL equation; however, constructing those solutions for double-fluxoid vortex lattices in terms of the $a_{\mathbf{K}}$ is not trivial, either, and we detail our method in Appendix C below.

In order to have a finite computational problem the expansions for ω, b, and $\mathbf{q}$ must be truncated; and the iterations involve integrals over the unit cell which must be numerically evaluated. These two issues are related. For single-fluxoid lattices it was sufficient to carry out the quadrature by summation of values on a grid aligned with the primitive lattice vectors, and to include in the expansions only $|\mathbf{K}|\le K_{\max}$ with $K_{\max}$ chosen so that the number of reciprocal lattice vectors was about the same as the number of points in the integration grid. For double-fluxoid lattices the situation is more complicated.

The expansion [Eq. (B2)] for ω can be rearranged so that it has nearly the same form as for single-fluxoid lattices

$$\omega(\mathbf{r})=\sum_{\mathbf{K}}\left[2a_{\mathbf{K}}-\frac{1}{2}a_{\mathbf{K}/2}\right][1-\cos(\mathbf{K}\cdot\mathbf{r})]. \tag{B7}$$

Equations (B1), (B2), and (B7) are identical for infinite sums but they are different when truncated. As discussed in Appendix C, the $a_{\mathbf{K}}$ that solve the linearized GL equations for double-fluxoid lattices do not fall off in a Gaussian manner like they do for single-fluxoid lattices; however, it turns out that $2a_{\mathbf{K}}-\frac{1}{2}a_{\mathbf{K}/2}$ is nearly Gaussian. This motivates the following truncation scheme for constructing ω when evaluating integrals: use Eq. (B7), including in the sum reciprocal lattice vectors with $|\mathbf{K}|\le K_{\max}$ except for fundamentals with $K_{\max}/2<|\mathbf{K}|\le K_{\max}$. Expressions analogous to Eq. (B7) exist for b and $\mathbf{q}$, and we apply the same truncation scheme when calculating them for the purposes of numerical integration and graphical display. Failure to use this truncation scheme, and instead simply cutting off the sums in Eqs. (B1), (B3), and (B4) with the condition $|\mathbf{K}|\le K_{\max}$, leads to high wave number artifacts. These artifacts generate a negative ω near the vortex core, which allows the ωQ^2 term in the free energy to become negative and quickly leads the iterations to run away.

It is tempting to define $c_{\mathbf{K}}\equiv 2a_{\mathbf{K}}-\frac{1}{2}a_{\mathbf{K}/2}$, $d_{\mathbf{K}}\equiv 2b_{\mathbf{K}}-\frac{1}{2}b_{\mathbf{K}/2}$, and carry out iterative calculations for those quantities, by moving the $\frac{1}{4}a_{\mathbf{K}/2}$ from the right side of Eq. (B5) to the left [and likewise for Eq. (B6)]. The resulting equations have exactly the form of Eqs. (11) and (13) from Ref. 27 for the iterations of the coefficients for single-fluxoid lattices. Doing this invariably leads to single-fluxoidlike solutions (behaving like $\omega\sim r^2$ and $B(0)-B(r)\sim r^2$ near the vortex core) which are inconsistent with the assumed forms of $\bar{B}$, $\mathbf{Q}_A$, and S. These unphysical solutions are free energy saddle points rather than minima.

APPENDIX C: SOLVING THE LINEARIZED GL EQUATIONS IN TERMS OF THE $a_{\mathbf{K}}$

In his pioneering work on vortex lattices in superconductors, Abrikosov[21] showed that for an applied field just below H_{c2}, the first GL equation (when expressed as an equation for the order parameter) has the form of Schrödinger's equation for a charged particle confined to a plane and subject to a magnetic field. With an assumed periodicity of the vortex lines and one flux quantum per vortex, an analytic solution ψ_A exists and can be expressed[21,34,35] in terms of a Jacobi theta function,

$$\psi_A(x,y)=e^{-\pi y^2/x_1y_2}\vartheta_1\left[\frac{\pi}{x_1}(x+iy),\frac{x_2+iy_2}{x_1}\right], \tag{C1}$$

where the lattice parameters x_1, x_2, and y_2 were defined just below Eq. (B4). This leads[18] to the Fourier-like expansion $\omega_A=\Sigma_{\mathbf{K}}a^A_{\mathbf{K}}[1-\cos(\mathbf{K}\cdot\mathbf{r})]$, with $a^A_{\mathbf{K}}=-(-)^{m+mn+n}e^{-K^2_{mn}S/8\pi}$.

Lasher[36] pointed out that for vortices of multiplicity p, $\psi^{(p)}_A(r)=[\psi_A(r/\sqrt{p})]^p$ is a corresponding solution of the linearized GL equations. In principle one could use this form to determine $a^A_{\mathbf{K}}$ for double-fluxoid lattices in Eq. (B1), starting from Eq. (C1), but we did not attempt to carry that through.

We have taken an alternative approach based on numerical solution of a linear system for the $a^A_{\mathbf{K}}$ derived from the linearized GL equations. In the linear regime $b(\mathbf{r})=B(0)-\bar{B}-\omega_A(\mathbf{r})/2\kappa$ (see, for example, De Gennes,[37] Sec. 6.7). Taking the curl and combining with the second GL equation yields

$$\frac{1}{2\kappa}\nabla\omega_A\times\hat{\mathbf{z}}=\omega_A\mathbf{Q}_A. \tag{C2}$$

Combining Eqs. (B2) and (C2), and the Fourier expansion for the supervelocity in the Abrikosov limit [see Eq. (24) in Ref. 18], leads to the linear system

$$\sum_{\mathbf{K}_i}A_{ji}a^A_{\mathbf{K}_i}=-\langle\omega_A\rangle \tag{C3}$$

with

$$A_{ji}\equiv C_{ji}-\delta_{\mathbf{K}_i,\mathbf{K}_j}\frac{1}{2\bar{B}\kappa}|\mathbf{K}_j|^2+\delta_{\mathbf{K}_i,\mathbf{K}_j/2}\frac{1}{8\bar{B}\kappa}|\mathbf{K}_j|^2 \tag{C4}$$

and

$$C_{ji}\equiv-\frac{|\mathbf{K}_j|^2-\mathbf{K}_i\cdot\mathbf{K}_j}{|\mathbf{K}_j-\mathbf{K}_i|^2}-\frac{|\mathbf{K}_j|^2+\mathbf{K}_i\cdot\mathbf{K}_j}{|\mathbf{K}_j+\mathbf{K}_i|^2}+\frac{|\mathbf{K}_j|^2-2\mathbf{K}_i\cdot\mathbf{K}_j}{4|\mathbf{K}_j-2\mathbf{K}_i|^2}+\frac{|\mathbf{K}_j|^2+2\mathbf{K}_i\cdot\mathbf{K}_j}{4|\mathbf{K}_j+2\mathbf{K}_i|^2}. \tag{C5}$$

We follow Brandt's convention that $\langle\omega_A\rangle=1$, so $(3/2)\Sigma_{\mathbf{K}}a^A_{\mathbf{K}}=1$.

The system of Eq. (C3) could be rendered finite by setting $a^A_{\mathbf{K}}=0$ for $|\mathbf{K}|>K_{\max}$; however, this is not a good closure assumption because of slow convergence with increasing $K_{\max}$. Equation (C4) shows the strong connection between $a^A_{\mathbf{K}}$ and $a^A_{\mathbf{K}/2}$ mentioned in Appendix B. For $K_{\max}/2<|\mathbf{K}|\le K_{\max}$ the corresponding $a^A_{\mathbf{K}}$ are connected to coefficients associated with vectors beyond the cutoff. In addition, as $|\mathbf{K}_j|\to\infty$, $C_{ji}\to-3/2$, which leads via Eq. (C4) to $a^A_{\mathbf{K}}\approx a^A_{\mathbf{K}/2}/4$ at large $|\mathbf{K}|$. We therefore set $a^A_{2\mathbf{K}}=a^A_{\mathbf{K}}/4$, $a^A_{4\mathbf{K}}=a^A_{\mathbf{K}}/16$, and so on for $K_{\max}/2<|\mathbf{K}|\le K_{\max}$, which leads to a modified linear system with coefficients A'_{ji}. For $|\mathbf{K}_i|\le K_{\max}/2$, $A'_{ji}=A_{ji}$ but for $K_{\max}/2<|\mathbf{K}_i|\le K_{\max}$,

$$A'_{ji}=A_{ji}+\sum_{l=1}^{\infty}4^{-l}C_{j,2^li}. \tag{C6}$$

In the numerical calculations we have truncated the sum at $l=4$ after finding no significant change in the $a^A_{\mathbf{K}}$ when further terms are included.

As a check on this approach to solving the linearized GL equations we have carried an analogous analysis for single-fluxoid lattices. The numerical results from solving the corresponding linear equations for the $a^A_{\mathbf{K}}$ match the analytic expression.

APPENDIX D: SOLVING THE GL EQUATIONS FOR DOUBLE-FLUXOID VORTEX LATTICES IN FILMS

The Ansätze for the various physical quantities are

$$\omega(\mathbf{r})=\sum_{\mathbf{K}_\perp,K_z}\left[2a_{\mathbf{K}_\perp K_z}-\frac{1}{2}a_{\mathbf{K}_\perp/2,K_z}\right][1-\cos\mathbf{K}_\perp\cdot\mathbf{r}_\perp]\cos K_zz, \tag{D1}$$

$$\mathbf{q}(\mathbf{r})=\sum_{\mathbf{K}_\perp,l}\left[2b_{\mathbf{K}_\perp l}-\frac{1}{2}b_{\mathbf{K}_\perp/2,l}\right]\frac{\hat{\mathbf{z}}\times\mathbf{K}_\perp}{K_\perp^2}\sin\mathbf{K}_\perp\cdot\mathbf{r}_\perp P_{2l}(2z/d), \tag{D2}$$

$$b_z(\mathbf{r})=\sum_{\mathbf{K}_\perp,l}\left[2b_{\mathbf{K}_\perp l}-\frac{1}{2}b_{\mathbf{K}_\perp/2,l}\right]\cos\mathbf{K}_\perp\cdot\mathbf{r}_\perp P_{2l}(2z/d), \tag{D3}$$

$$\mathbf{b}_\perp(\mathbf{r})=\sum_{\mathbf{K}_\perp,l}\left[2b_{\mathbf{K}_\perp l}-\frac{1}{2}b_{\mathbf{K}_\perp/2,l}\right]\frac{-\mathbf{K}_\perp}{K_\perp^2}\sin\mathbf{K}_\perp\cdot\mathbf{r}_\perp\frac{2}{d}P'_{2l}(2z/d) \tag{D4}$$

with $a_{\mathbf{K}_\perp/2,K_z}$ and $b_{\mathbf{K}_\perp/2,l}$ vanishing if $\mathbf{K}_\perp/2$ is not a reciprocal lattice vector.

The iterative equation for $a_{\mathbf{K}_\perp K_z}$, replacing Eq. (A15), is

$$a_{\mathbf{K}_\perp K_z}:=\frac{2\langle(\omega^2-2\omega+\omega Q^2+g)\cos\mathbf{K}_\perp\cdot\mathbf{r}_\perp\cos K_zz\rangle_{\mathrm{U}}}{(\delta_{K_z,0}+1)[(K_\perp^2+K_z^2)/2\kappa^2+1]}+\frac{1}{4}a_{\mathbf{K}_\perp/2,K_z}. \tag{D5}$$

The iterative equation for $b_{\mathbf{K}_\perp l}$ involves several auxiliary quantities. Replacing Eq. (A19) is

$$S_{\mathbf{K}_\perp l}=\sum_{l'=0}^{l}\left(\frac{17}{4}b_{\mathbf{K}_\perp,l'}-b_{\mathbf{K}_\perp/2,l'}-\frac{1}{4}b_{2\mathbf{K}_\perp,l'}\right)2l'(2l'+1)+\sum_{l'=l+1}\left(\frac{17}{4}b_{\mathbf{K}_\perp,l'}-b_{\mathbf{K}_\perp/2,l'}-\frac{1}{4}b_{2\mathbf{K}_\perp,l'}\right)2l(2l+1) \tag{D6}$$

and replacing Eq. (A18) is the expression

$$D_{\mathbf{K}_\perp,l}=\left\langle\omega(\hat{z}\cdot\mathbf{K}_\perp\times\mathbf{Q})\left[4\sin(\mathbf{K}_\perp\cdot\mathbf{r}_\perp)-\frac{1}{2}\sin(2\mathbf{K}_\perp\cdot\mathbf{r}_\perp)\right]P_{2l}(2z/d)\right\rangle_{\mathrm{G}}. \tag{D7}$$

The stray-field coefficients, replacing Eq. (A17), are given by

$$b^s_{\mathbf{K}_\perp}=\sum_l 2b_{\mathbf{K}_\perp l}-\frac{1}{2}b_{\mathbf{K}_\perp/2,l}. \tag{D8}$$

Then the desired iterative equation, replacing Eq. (A21), is

$$b_{\mathbf{K}_\perp l}:=\frac{1}{1+c\langle\omega\rangle}\frac{4}{17}\left\{b_{\mathbf{K}_\perp/2,l}+b_{2\mathbf{K}_\perp,l}+\frac{17}{4}c\langle\omega\rangle b_{\mathbf{K}_\perp l}+\frac{4l+1}{K_\perp^2}\times\left[-2S_{\mathbf{K}_\perp l}/d^2-D_{\mathbf{K}_\perp l}-2K_\perp\left(2b^s_{\mathbf{K}_\perp}-\frac{1}{4}b^s_{2\mathbf{K}_\perp}\right)/d\right]\right\}. \tag{D9}$$

The discussion in Appendix B concerning truncation schemes for the sums representing ω, $\mathbf{b}$, and $\mathbf{q}$ is equally germane in film geometry.

*martin.gelfand@colostate.edu

[1] M. Tinkham, Phys. Rev. **129**, 2413 (1963).
[2] K. Maki, Ann. Phys. (N.Y.) **34**, 363 (1965).
[3] G. Lasher, Phys. Rev. **154**, 345 (1967).
[4] D. J. E. Callaway, Ann. Phys. (N.Y.) **213**, 166 (1992).
[5] J. Pearl, Appl. Phys. Lett. **5**, 65 (1964).
[6] J. Pearl, Ph.D. thesis, Polytechnic Institute of Brooklyn, 1965.
[7] G. J. Dolan and J. Silcox, Phys. Rev. Lett. **30**, 603 (1973).
[8] G. J. Dolan, J. Low Temp. Phys. **15**, 133 (1974).
[9] G. J. Dolan, J. Low Temp. Phys. **15**, 111 (1974).
[10] S. Hasegawa, T. Matsuda, J. Endo, N. Osakabe, M. Igarashi, T. Kobayashi, M. Naito, A. Tonomura, and R. Aoki, Phys. Rev. B **43**, 7631 (1991).
[11] G. S. Mkrtchyan and V. V. Shmidt, Sov. Phys. JETP **34**, 195 (1972).
[12] G. R. Berdiyorov, M. V. Milosević, and F. M. Peeters, Phys. Rev. Lett. **96**, 207001 (2006).
[13] V. A. Schweigert, F. M. Peeters, and P. S. Deo, Phys. Rev. Lett. **81**, 2783 (1998).
[14] G. R. Berdiyorov, A. D. Hernandez, and F. M. Peeters, Phys. Rev. Lett. **103**, 267002 (2009).
[15] V. V. Moshchalkov, X. G. Qiu, and V. Bruyndoncx, Phys. Rev. B **55**, 11793 (1997).
[16] E. B. Bogomol'nyi, Sov. J. Nucl. Phys. **24**, 449 (1976).
[17] I. Luk'yanchuk, Phys. Rev. B **63**, 174504 (2001).
[18] E. H. Brandt, Phys. Status Solidi B **51**, 345 (1972).
[19] E. H. Brandt, Phys. Rev. B **71**, 014521 (2005).
[20] J. Matricon, Ph.D. thesis, Université de Paris, 1966.
[21] A. A. Abrikosov, Sov. Phys. JETP **5**, 1174 (1957).
[22] D. J. Priour and H. A. Fertig, Phys. Rev. B **67**, 054504 (2003).
[23] D. J. Priour and H. A. Fertig, Phys. Rev. Lett. **93**, 057003 (2004).
[24] R. Prozorov, A. F. Fidler, J. R. Hoberg, and P. C. Canfield, Nat. Phys. **4**, 327 (2008).
[25] R. Prozorov, R. W. Giannetta, A. A. Polyanskii, and G. K. Perkins, Phys. Rev. B **72**, 212508 (2005).
[26] R. E. Goldstein, D. P. Jackson, and A. T. Dorsey, Phys. Rev. Lett. **76**, 3818 (1996).
[27] E. H. Brandt, Phys. Rev. Lett. **78**, 2208 (1997).
[28] U. Klein and B. Pöttinger, Phys. Rev. B **44**, 7704 (1991).
[29] M. M. Doria, J. E. Gubernatis, and D. Rainer, Phys. Rev. B **39**, 9573 (1989).
[30] A. B. Pippard, Philos. Mag. **19**, 217 (1969).
[31] J. Hove, S. Mo, and A. Sudbo, Phys. Rev. B **66**, 064524 (2002).
[32] E. H. Brandt, Phys. Status Solidi **36**, 381 (1969).
[33] M. Tinkham, *Introduction to Superconductivity*, 2nd ed. (McGraw Hill, New York, 1996), p. 454.
[34] W. H. Kleiner, L. M. Roth, and S. H. Autler, Phys. Rev. **133**, A1226 (1964).
[35] E. H. Brandt, Phys. Status Solidi B **36**, 393 (1969).
[36] G. Lasher, Phys. Rev. **140**, A523 (1965).
[37] P.-G. de Gennes, *Superconductivity of Metals and Alloys* (W. A. Benjamin, New York, 1966), p. 274.